Journal of the Korean Chemical Society
2018, *Vol. 62, No. 1*
Printed in the Republic of Korea
https://doi.org/10.5012/jkcs.2018.62.1.7

Synthesis, Characterization and Catalytic Evaluation of Zinc Fluorides for Biodiesel Production

Sus Indrayanah, I Nyoman Marsih†, and Irmina Kris Murwani*

Jurusan Kimia, Institut Teknologi Sepuluh Nopember Kampus ITS Sukolilo-Surabaya 60111, Indonesia.
†Jurusan Kimia, Institut Teknologi Bandung Kampus ITB JL. Ganesha 10-Bandung 40132, Indonesia.
**E-mail: irmina@chem.its.ac.id*
(Received September 8, 2017; Accepted December 3, 2017)

ABSTRACT. The potential of zinc fluorides with different molar ratios of Zn/F was applied as a solid catalyst in the simultaneous reaction of transesterification and esterification of crude palm oil (CPO) for biodiesel production. These materials were prepared by the fluorolytic sol-gel technique with different fluorine contents. The resulting samples were investigated using elemental analysis, XRD, FT-IR, TG/DTG, N_2 physisorption measurements and SEM. The results exhibited that the presence of fluorine strongly affected the catalytic activity in the biodiesel production. The catalysts with smaller fluorine contents (≤1) showed the best performance in all of the observed samples, yields from 92.94 to 89.95, 87.38 and 85.21% with increasing fluorine contents, respectively. The yield toward the formation of biodiesel depended on the phase and particle sizes of catalysts, but it was not influenced by surface area, pore size, and volume of the samples. The recovered catalyst showed a gradual decrease in activity over three cycles of same reactions.

Key words: Zinc fluoride, Sol-gel method, Heterogeneous catalyst, Biodiesel, Crude palm oil (CPO)

INTRODUCTION

In the past years, biodiesel became one of the most attractive alternatives to fossil fuels because it exhibited some advantages such as high biodegradability, nontoxicity, renewability, higher flash point, high octane number, and good lubricity.[1] Due to environmental issues such as air pollution and global warming associated with the burning of fossil fuels, the demand for biodiesel as a replacement for petroleum-based fuels has increased.[2] Biodiesel, that is, alkyl esters of long chain fatty acids could be obtained through catalytic transesterification reactions of renewable feedstocks such as vegetable oils or animal fats with alcohol in the presence of a base catalyst.[3]

Base catalysts such as NaOH or KOH inhomogenous phase were widely used in industrial scale for the production of biodiesel because of their higher catalytic activity than acid catalysts.[4-5] However, the base catalysts are susceptible to triglycerides containing high free fatty acids (FFA) and water. The existence of FFA and water caused soap formation, damaging the catalytic activity. Therefore, acid-catalyzed reactions are suitable for the vegetable oils containing higher FFA and water since acid catalysts are robust against FFA, a constituent of renewable feedstocks.[6] In fact, many types of homogeneous acid catalysts such as H_2SO_4, HCl and H_3PO_4 are used in the biodiesel production.[7,8] Nevertheless, these catalysts tend to show lower activities and thus require a longer reaction time. Moreover, the acid-catalyzed reactions get the drawback of being highly corrosive. Therefore, the use of solid acid catalysts in heterogeneous phase for the production of biodiesel can be an alternative to minimize harmful impact on the environment.[9]

Since solid acid catalysts in the biodiesel production was less corrosive, reusable, and water-tolerant,[10] they were applied for biodiesel production in a one-step process, known as the simultaneous reaction of transesterification and esterification. Many researchers reported the successful replacement of conventional homogeneous system by heterogeneous catalysts like ion-exchange resins, Amberlyst-15 and Nafion,[11,12] zirconium based catalysts,[13,14] heteropoly acids,[15,16] and zeolites.[17,18] However, these catalysts showed some disadvantages such as the inactivity under high-temperature reactions (resin), mass transfer limitation and deactivation (zeolite), and loss of activity in polar solvents due to high solubility (heteropoly acid).

Recently, fluoride-based material like magnesium fluoride has been used as a solid catalyst in some reactions such as synthesis of vitamin E,[19] vitamin K,[20] benzylation of benzene,[21] and acetylation of glycerol.[22] The performance of this material is known to be associated with the structures, surface areas, tuneable acidity and mesopore sizes.[23]

Since magnesium fluoride exhibited high catalytic performance of in various reactions, zinc fluoride can be suggested as an attractive alternative due to its structural similarity to magnesium fluoride. Additionally, the properties of Mg and Zn ions are proportional to each other in the oxidation state and ionic radii.[24]

Consequently, we here report the synthesis, characterisation, and application of zinc fluorides having different Zn/F ratios as a heterogeneous catalyst for production of biodiesel. They were synthesized according to the fluorolytic sol-gel method using 48% aqueous HF. The molar ratios of Zn/F of the samples could be adjusted by the various 48% aqueous HF from 0.5 to 2. Furthermore, all samples obtained from the sol-gel method were characterized by X-ray diffraction, FT-IR, TG/DTG, N_2 adsorption-desorption, and SEM to get information about the crystal structure, chemical bonding, thermal behavior, surface area, porosity, and morphology of the samples.

The performance of the resulting samples with different Zn/F molar ratios were tested as a heterogeneous catalyst in the production of biodiesel via the simultaneous reaction of transesterification and esterification between crude palm oil (CPO) and methanol. The activity of the catalyst was calculated based on the biodiesel obtained. Moreover, to evaluate the durability or lifetime the catalyst, the same catalyst was used under absolutely equal reaction conditions.

EXPERIMENTAL

Synthesis of catalysts

The zinc fluorides with different molar ratios of Zn/F were synthesized by a sol-gel method. In the first step, zinc acetate, $Zn(CH_3COO)_2 \cdot 2H_2O$ (99.98% powder) was dissolved in methanol. Then the amount of aqueous hydrofluoric, 48% wt.-HF was added and stirred at about 400 rpm. The stoichiometry of the zinc fluoride phases can be easily adjusted by the molar proportion of HF, which was varied between. The produced sol or gel was aged for 12 h and then the solvent was removed under vacuum. Finally, the resulting materials were dried under vacuum for 5 h at 70 °C.

Characterization of catalyst

The elemental analysis (C, H, N contents) were determined using a CHNS analyser. The fluoride content was determined by means of ion chromatography with conductivity detector. The zinc contents of the materials were determined by the ICP-OES. The XRD patterns of the materials in this work were obtained using a Philips X-Pert X-ray diffractometer (λ = 1.54056 Å) at 2θ = 20-80°. The FT-IR spectra of the samples prepared by a sol-gel technique were recorded on a Shimadzu spectrometer equipped with KBr windows in the range of 4000-400 cm^{-1}. The thermal analysis (TG/DTG) was performed in N_2 atmosphere with a METTLER TOLEDO apparatus fitted with a Pt/PtRh10 thermocouple. The porosity characteristics of the powder were examined by the N_2 adsorption-desorption isotherms measured on a Micromeritics Quantachrome Instrument. The SEM images of all samples were obtained using ZEISS EVO MA 10. The biodiesel obtained from the catalytic reactions was analyzed with an HP6890 GC chromatograph equipped a FID detector: oven temperature = 140 °C, injector temperature = 200 °C and detector temperature = 250 °C.

Catalytic tests

The performance of the samples obtained from a sol-gel method was evaluated by the simultaneous reaction of transesterification and esterification between CPO and methanol in a Teflon-lined autoclave. First, the reactor was charged with 10 g of CPO and 48 mL methanol, which corresponds to a 1:30 molar ratio of CPO/methanol, and 0.5 g catalyst (5% of CPO). Then, the reaction mixture was heated at 150 °C (oil bath) under constant stirring (600 rpm) for 5 hours. After that, the mixture was cooled to room temperature, and the catalyst was separated by centrifugation. The residual methanol was removed with a rotary evaporator and methyl esters was analyzed by gas chromatography (GC). The biodiesel yield was calculated using the equation employed by Li et al.[25]

In this work, the lifetime or durability of the catalyst was essential. Therefore, to study the stability of the catalyst, the simultaneous reaction of transesterification and esterification between CPO and methanol was conducted under the same reaction conditions and catalyst: CPO to methanol molar ratio of 1:30 at temperature 150 °C for 5 hours with 0.5 g catalyst and stirring speed 600 rpm. After the reaction finished, the catalyst was separated and washed with ethanol, acetone, and distilled water to remove impurities, and used for the subsequent runs.

RESULTS AND DISCUSSION

The results of elemental analysis (wt %), respective composition of zinc fluoride synthesized with the 48 wt % HF and various molar ratios of Zn/F are summarized in *Table* 1. The theoritical elemental contents for Zn and F in

***Table* 1.** Result of elemental analyses of samples prepared with 48 wt % HF and different Zn/F ratios

Zn/F ratios	Element (%)			
	Zn	F	C	H
1:0.5	48.98	5.79	12.81	5.62
1.1	40.46	11.06	18.40	1.85
1:1.5	50.25	20.81	11.67	1.05
1:2	50.25	28.87	2.50	1.40

*Calculated composition: $Zn_{0.75}F_{0.30}(CH_3COO)_{0.53}(OH)_{0.66}(H_2O)_{1.20}$: Zn = 48.98%, F = 5.79%, C = 12.81%, H = 5.62%; $Zn_{0.62}F_{0.58}(CH_3COO)_{0.66}(CH_3OH)_{0.21}(H_2O)_{0.46}$: Zn = 40.46%, F = 11.06%, C = 18.40%, H = 1.85%; $Zn_{0.77}F_{1.10}(CH_3COO)_{0.44}(CH_3OH)_{0.09}(H_2O)_{0.08}$: Zn = 50.25%, F = 20.81%, C = 11.67%, H = 1.05%; $Zn_{0.77}F_{1.52}(CH_3OH)_{0.21}(OH)_{0.02}(H_2O)_{0.66}$: Zn = 50.25%, F = 28.87%, C = 2.50%, H = 1.40%.

ZnF_2 are 63 and 37%, respectively.[26] Although various molar ratios of Zn to F were applied in the sol gel synthesis, the F contents in the resulting samples were lower than that pure ZnF_2. As given in *Table* 1, the carbon content decrease with the increasing of HF, showing the complete hydrolysis of zinc methoxide by water, especially zinc fluoride with molar ratios of Zn/F = 1:2. Based on the the mass percentages of Zn, F, C, and H in the prepared samples, the final composition of these materials corresponds to the equivalents of HF used for the synthesis as presented in *Table* 1.

The X-ray diffraction patterns of the zinc fluoride phases with different molar ratios of Zn/F are displayed in *Fig.* 1. The XRD patterns for samples with various Zn/F ratios show, expectedly, the diffraction of pure ZnF_2 (peaks at 2θ = 26.69°, 34.39°, 39.88°, 52.98° and 61.92° indicated by ♦). Interestingly enough, even the phase with the nominal composition of Zn/F ratios (1:1.5) still adapts the structure of pure ZnF_2 as was also observed for the $Mg(OH)_{2-x}F_x$-system. Starting with the nominal composition Zn/F (1:1), in addition to the ZnF_2 peaks, which still are present, typical peaks for Zn acetate appear at 2θ = 22.83 and 24.19 (marked with ♠). These peaks slightly developed further for the nominal sample Zn/F ratios (1:0.5). Thus, the XRD patterns of these samples prepared by the sol-gel method indicate the dominating presence of the ZnF_2-structure type over a wide range (Zn/F<1), only with lower F-stoichiometries (Zn/F>1) additional reflections of the Zn acetate structure type become visible.

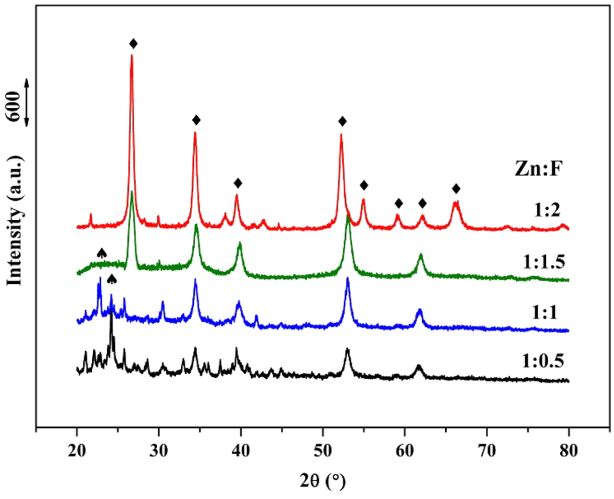


***Figure* 1.** XRD patterns of zinc fluorides with different Zn/F ratios.

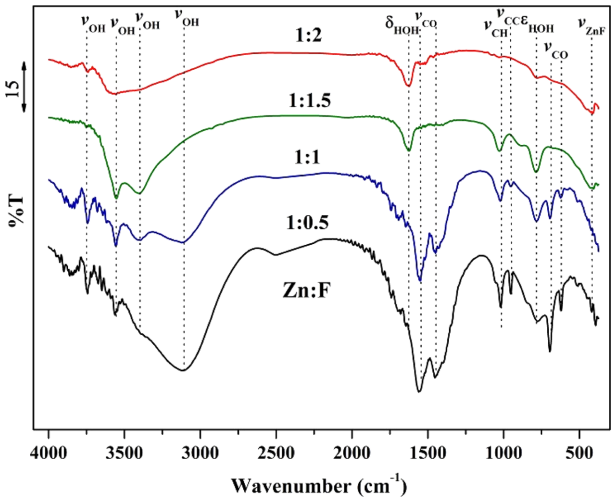


***Figure* 2.** FT-IR spectra of zinc fluorides with different Zn/F ratios.

The Fourier transform infrared (FT-IR) investigations are in line with the XRD results. *Fig.* 2 shows the FTIR spectra of zinc fluorides with different Zn/F ratios. The bands at 3000-3700 cm^{-1} present adsorbed H_2O molecules and bridging OH groups as well. The existence of adsorbed water is also shown by the spectral bands located at 1640 and 790 cm^{-1}, respectively. Moreover, the band at 3711 cm^{-1} demonstrate nonbridging OH groups. Expectedly, it decreases with increasing fluorine contents. Based on the FTIR results, the presence of Zn-OH moieties in all samples has been verified. The bands about 1563, 1453, 702 and 615 cm^{-1} are attributed to acetate groups, and these bands decrease with higher F-stoichiometries (Zn/F<1). The spectra located about 1030 and 950 cm^{-1} in resulting materials indicate the stretching vibration of C-O and C-C bonds. These spectra decrease with increasing fluorine contents. This result shows that zinc fluoride with a different molar ratio of Zn/F (1:2) does not have residual acetate groups or methanol. The Zn-F bond is well characterized by the band at 418 cm^{-1}.

The thermal behavior of the samples, especially the effect of fluorine is examined by TG/DTG. The TG/DTG curves

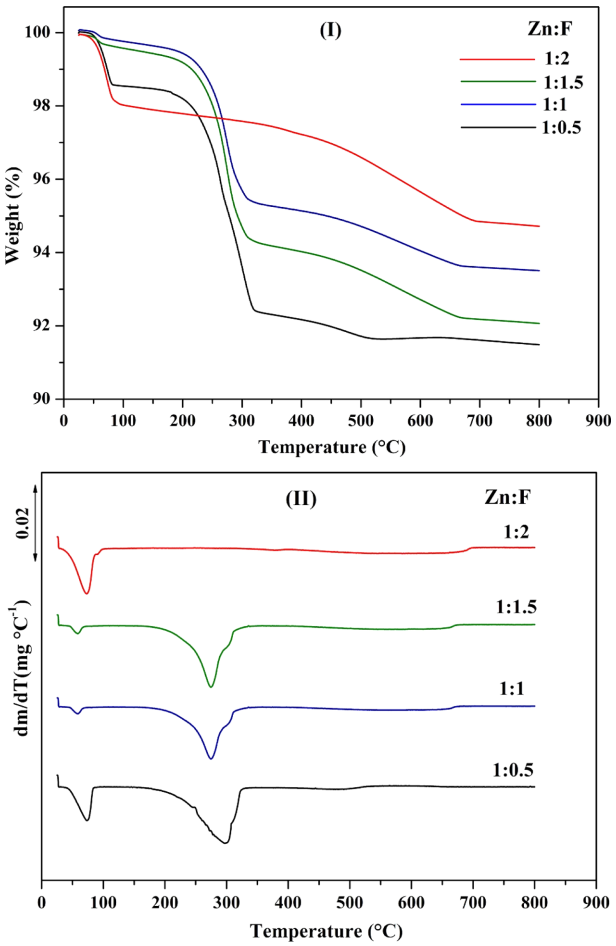


***Figure* 3.** TG (I) and DTG (II) curves of zinc fluorides with different Zn/F ratios.

of zinc fluoride with different Zn/F ratios are presented in *Fig.* 3 (I and II). As shown in *Fig.* 3, TG/DTG curves demonstrated that all materials obtained from the sol-gel method have the similar destructive phase, except pure ZnF_2. The TG curve in *Fig.* 3I. indicates two distinct temperature regions of mass losses. The first temperature zone between 80 and 100 °C is associated with the removal of physisorbed water and traces of adsorbed methanol. In the temperature between 250 and 320 °C, both a significant thermal decomposition and release of acetate groups took place. The sample with a molar ratio of Zn/F (1:2) does not contain any unconverted acetate groups. Hence, no mass loss in the temperature between 250-320 °C occurs. Expectedly, all samples with under-stochiometric F-containing phases exhibit two decomposition regions characterized by water release (adsorbed H_2O and/or OH-condensation) and decomposition of unconverted acetate groups at a higher temperature. Thus, these results are in line with those deduced

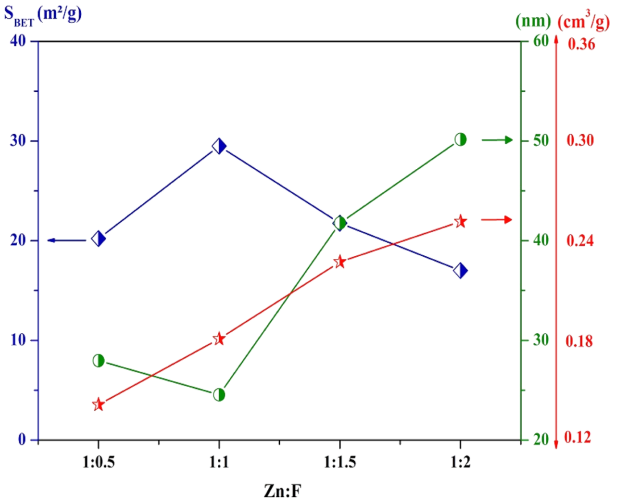


***Figure* 4.** Surface area$_{(BET)}$ (◆), average pore size (◑) and volume (★) of zinc fluorides with different Zn/F ratios.

from XRD and FTIR investigations. Decomposition and removal of HF were not observed, indicating that the Zn-F bonds in these materials are thermally robust.

The influence of the amount of fluorine on the surface area$_{(BET)}$ of the resulting samples is displayed in *Fig.* 4. Based on the N_2 adsorption-desorption results, the surface area (◆) increases with increasing fluorine contents. However, by adding fluorine contents ≥1.5, the surface area of sample decreases. All samples show the relatively small surface area of 30 m^2/g. However, these materials are very active as heterogeneous catalysis for biodiesel production (will be explained in the catalytic test). The decreasing of surface area$_{(BET)}$ is caused by the reduction of OH groups and methoxide residue of the samples. Not only the surface area but also the average pore size (◑) and volume (★) can also be calculated from the N_2 adsorption-desorption as described in *Fig.* 4. Contras of surface area, in *Fig.* 4 shows that the average pore size decreases with increasing fluorine contents, but by adding fluorines ≥1.5, the pore size of these samples increases. Moreover, pore volume increases with increasing fluorine contents. The decreasing of average pore size is always accompanied by an increase of surface area of the sample. The average pore size of the resulting materials about 27.97-50 nm, while its pore volume ranges from 0.14 to 0.26 cm^3/g, which lies in the mesopore range (≤50 nm). It is clear that there are smaller pores in all samples.

The porosity of the resulting materials was measured by N_2 adsorption-desorption. All samples have the same isotherm as shown in *Fig.* 5. The adsorption of nitrogen molecules begins to occur at P/P_0 from 0 to <0.1. Interaction

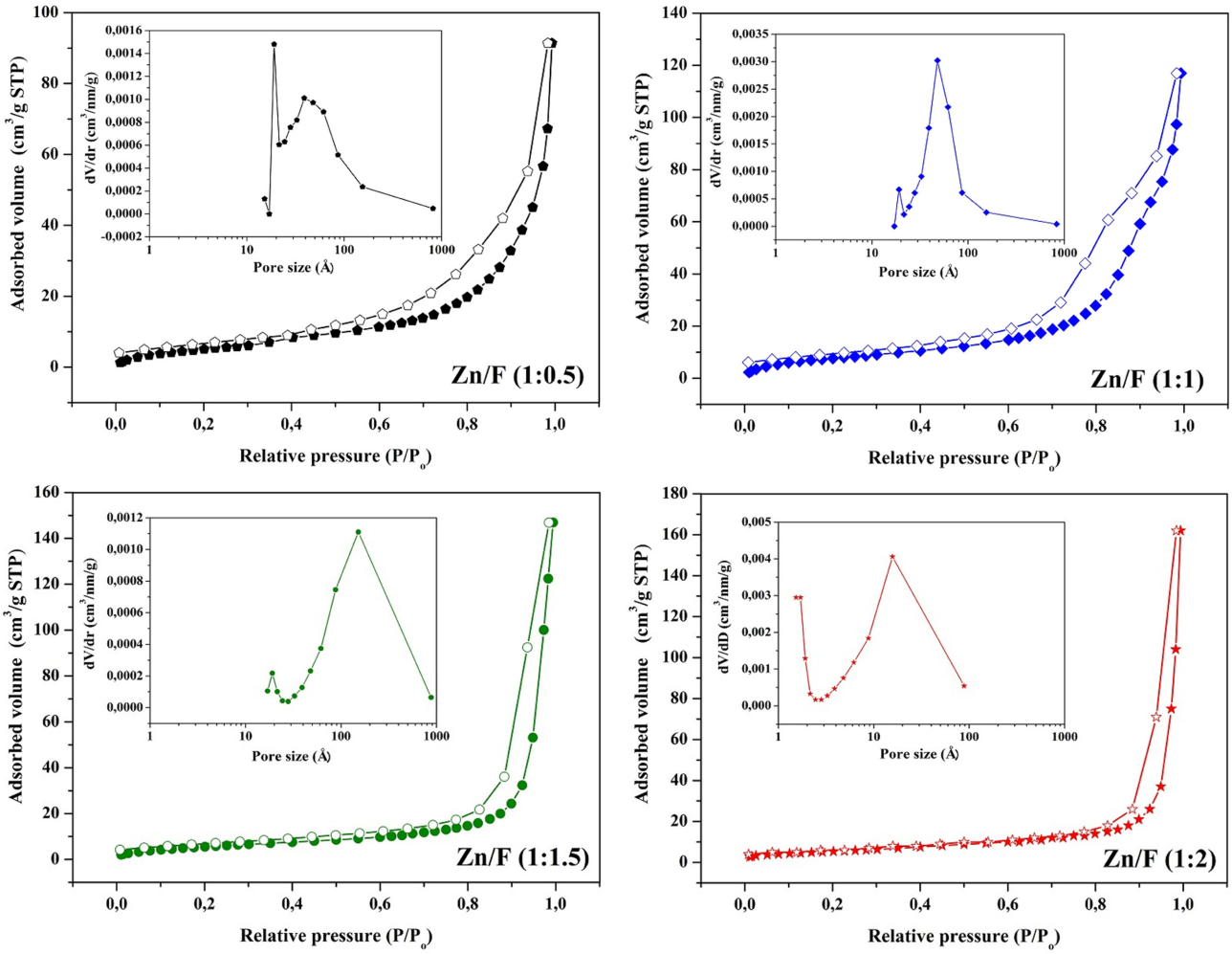


***Figure* 5.** The N_2 adsorption-desorption isotherms and the pore size distribution curves of zinc fluorides with different Zn/F ratios.

of nitrogen molecules adsorbed in the pores appears at P/P_0 about 0.4 that face each other, while at higher pressure (P/P_0 about 1), the isotherm curves rise sharply. This indicated that the pressure of the nitrogen molecules adsorbed is very large. Furthermore, at the pressure where desorption begins, the isotherm curves show hysteresis because of the capillary condensation of nitrogen molecules. Based on the IUPAC classification, the N_2 adsorption-desorption isotherms in *Fig.* 5 show the mesoporous features. With increasing fluorine contents, the isotherm curves are similar to that for the sample with lower fluorine content. The samples have typical II Brunauer isotherms that show the presence of macroporosity with a type H3 hysteretic loop. According to Mikhail and Robens, an H3 hysteretic loop is indicative of non-uniform pores. However, All samples present various porous characteristics as described in *Fig.* 4, which lies in the mesopore range (≤50 nm).

The scanning electron microscopy (SEM) was performed to investigate the topography and texture of resulting samples. *Fig.* 6 shows the images of these samples synthesized from sol-gel technique with different fluorine contents. It can be seen that the morphology of the synthesized samples is dissimilar from that of the sample with lower fluorine content. The shape of the particles reveals the uniform and more homogeneous with increasing fluorine content. The particle shapes also change from spired to more spherical with increasing fluorine contents. Furthermore, the greater of fluorine content, the larger of particle size. This result shows that the presence of fluorine can increase particle size. The particle size of these samples ranges from 50-100 nm.

The simultaneous reaction of transesterification and esterification between CPO and methanol for production of biodiesel was employed as a probe reaction to investigate the effect of fluorine contents. The reaction was evaluated under the same condition. Based on the previous experiment, the higher yield of biodiesel resulted from the

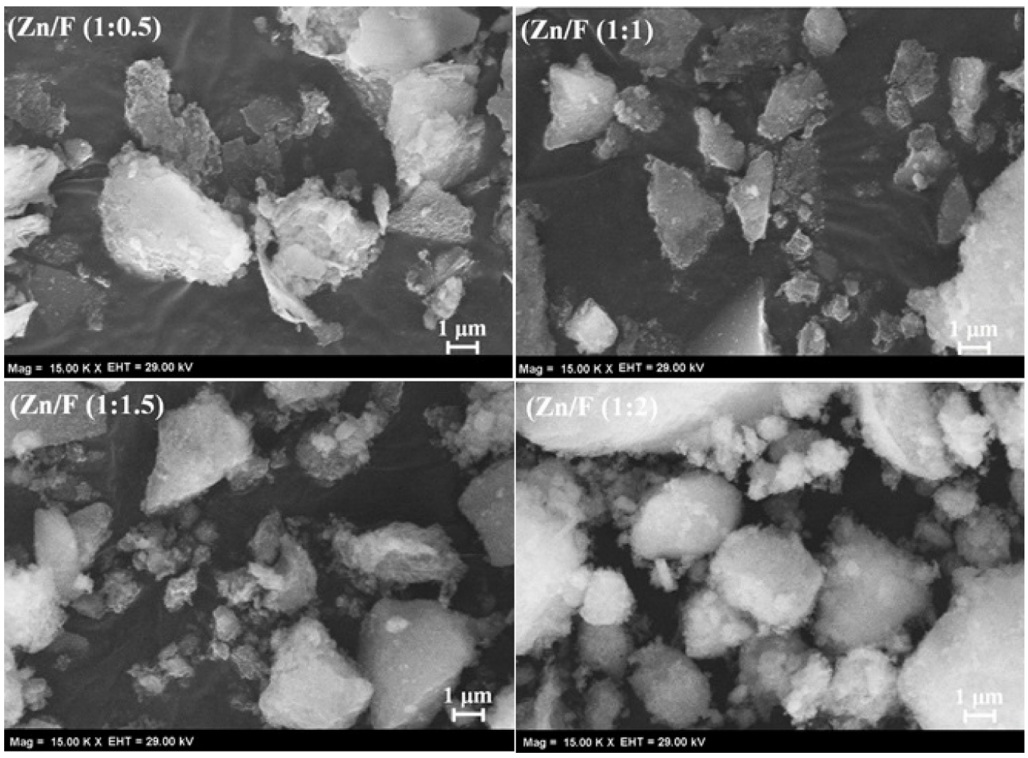


***Figure* 6.** SEM images of zinc fluoride with different Zn/F molar ratios.

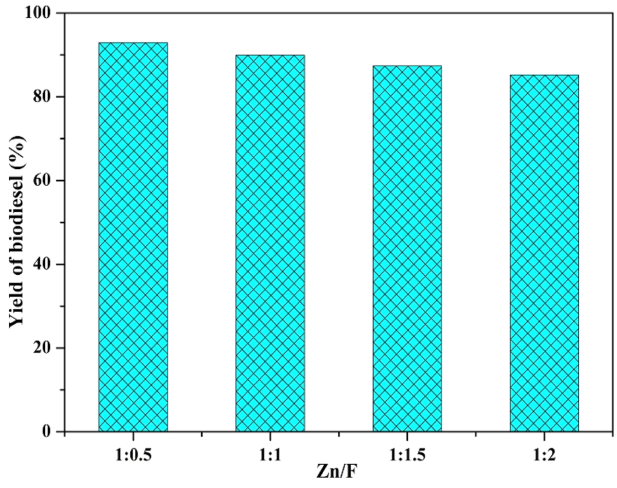


***Figure* 7.** The catalytic activity of zinc fluoride with different Zn/F ratios.

optimum condition (1:30 molar ratio of CPO/methanol at 150 °C under stirring speed 600 rpm for 5 h with catalyst/oil mass ratio of 5 wt %). Therefore, these parameters were used and the results are presented in *Fig.* 7. In summary, the catalytic activities of these four samples are dissimilar. The sample with a lower fluorine content demonstrates the highest biodiesel yield of 92.94%, but the yield of biodiesel decreases to 89.95, 87.38 and 85.21% with increasing fluorine contents, respectively. By adding fluorine contents ≥1.5, the catalysts come to have the larger pore size and volume (more abundant of mesopores), but the surface areas of these samples decrease. However, the larger pore size and volume of the samples with fluorine ≥1.5 cannot have sufficient contact between CPO and methanol because of their small surface areas.

Moreover, based on the data shown in *Fig.* 4, it shows that the sample with the lower fluorine content has the smallest surface area, pore size and volume when compared to other samples but it has the highest biodiesel yield. That is, the catalytic activity of the materials could not be related to surface areas, average pore size and pore volume. The XRD and SEM results imply that the samples with lower fluorine contents would have the best catalytic activity due to the active phase structure and the smaller particle sizes. The sample with lower fluorine contents (≤ 1) has an amorphous phase, which is more advantages than a crystal phase for biodiesel production. The amorphous phase and smaller particle size can provide more dispersed active sites, which helps to increase the contact between the active sites and reactants. In fact, the catalytic activity of the amorphous phase is better than the crystalline.

The reusability of the catalyst was also evaluated. After each reaction cycle, the used catalyst was recovered by

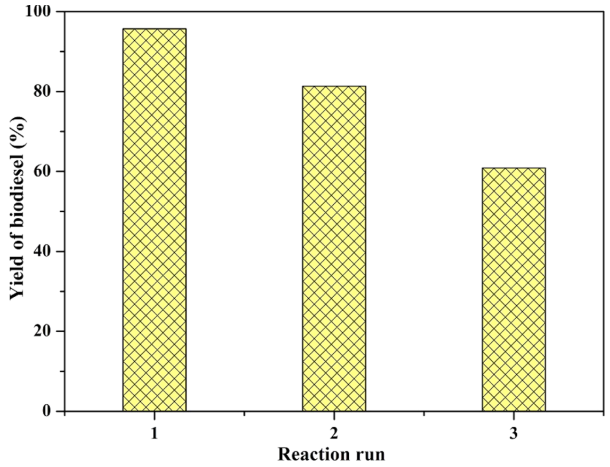


***Figure* 8.** The reusability of the catalyst. The experiments were investigated under the same reaction conditions and the catalyst. i.e Zinc fluoride with Zn/F (1:0.5).

centrifugation and washed with ethanol, acetone and distilled water. As shown in *Fig.* 8, the yield of biodiesel decreases over three runs from 92.94 to 60.88%, partly ascribed to a catalyst loss during the recovery process. In addition, the impurities such as fatty acid and byproducts such as glycerol might have blocked the pores of the catalyst.

CONCLUSION

The zinc fluorides with different molar ratios of Zn/F have been successfully synthesized by sol-gel processes and applied as a heterogeneous catalyst for the biodiesel production through simultaneous reactions of transesterification and esterification between CPO and methanol. The molar ratios of Zn to F can be easily controlled by simply adjusting the molar ratio of precursors of Zn acetate and 48 wt % HF. The catalysts with lower fluorine contents (≤1) showed the best performance in all of the observed samples, with the product yield from 92.94, 89.95, 87.38 and 85.21% with increasing fluorine contents, respectively. The yield of biodiesel depends on phase and particle sizes of catalysts, but it is not correlate to surface area, pore size and volume of the materials.

Acknowledgments. The authors thank to Directorate of Higher Education (DIKTI) and Pascasarjana Institut Teknologi Sepuluh Nopember (ITS) Indonesia for granting the scholarship and research grant for financial support.

REFERENCES

1. Soltani, S.; Rashid, U.; Al-Resayes, S. I.; Nehdi, I. A., *Energy Convers. Manag.* **2017**, *141*, 183.
2. Onoji, S. E.; Iyuke, S. E.; Igbafe, A. I.; Nkazi, D. B.; *Energy Convers. Manag.* **2016**, *110*, 125.
3. Helwani, Z., Aziz, N., Kim, J., Othman, M.R. *Renew. Energ.* **2016**, *86*, 68.
4. Likozar, B.; Pohar, A.; Levec, J. *Fuel Process. Technol.* **2016**, *142*, 326.
5. Goudarzi, M.B.; Boldor, D.; Nde, D. B. *Bioresour. Technol.* **2016**, *201*, 97.
6. Amani, H.; Asif, M.; Hameed, B. H. *J. Taiwan Inst. Chem. Eng.* **2016**, *58*, 226.
7. Rashed, M. M.; Kalam, M. A.; Masjuki, H. H.; Mofijur, M.; Rasul, M. G.; Zulkifli, N. W. M. *Depart. Ind. Crops Prod.* **2016**, *79*, 70.
8. Hidalgo, P.; Ciudad, G.; Mittelbach, M.; Navia, R. *Fuel* **2015**, *153*, 544.
9. Mohammed, N. I.; Kabbashi, N. A.; Alam, Md. Z.; Mirghani, M. E. S. *J. Taiwan Inst. Chem. Eng.* **2016**, *63*, 243.
10. Ezzah-Mahmudah, S.; Lokman, I. M.; Saiman, M. I.; Taufiq-Yap, Y. H. *Energy Convers. Manag.* **2016**, *126*, 124.
11. Fu, J.; Li, Z.; Xing, S.; Wang, Z.; Miao, C.; Lv, P.; Yuan, Z. *Fuel* **2016**, *181*, 1058.
12. Ma, Y.; Wang, Q.; Gao, Z.; Sun, X.; Wang, N.; Niu, R.; Ma, H. *Renew. Energ.* **2016**, *86*, 643.
13. Shi, G.; Yu, F.; Wang, Y.; Pan, D.; Wang, H.; Li, R. *Renew. Energ.* **2016**, *92*, 22.
14. Sani, Y. M.; Alaba, P. A.; Raji-Yahya, A. O.; AbdulAziza, A. R.; Daud, W. M. A. W. *J. Taiwan Inst. Chem. Eng.* **2016**, *59*, 195.
15. Han, Y. Z.; Hong, L.; Wang, X. Q.; Liu, J. Z.; Jiao, J.; Luo, M.; Fu, Y. J. *Ind. Crops Prod.* **2016**, *89*, 332.
16. Zhang, D. Y.; Duan, M. H.; Yao, X. H., Fu, Y. J.; Zu, Y. G. *Fuel* **2016**, *172*, 293.
17. Sani, Y. M.; Alaba P. A.; Raji-Yahya, A. O.; AbdulAziza A. R.; Daud, W. M. A. W. *J. Taiwan Inst. Chem. Eng.* **2016**, *60*, 247.
18. Vieira, S. S.; Magriotis, Z. M.; Ribeiro, M. F.; Graça, I.; Fernandes, A.; Lopes, J. M. F. M.; Coelho, S. M.; Santos, N. Ap. V.; Saczk, A. Ap. *Microporous and Mesoporous Material* **2015**, *201*, 160.
19. Wuttke, S.; Coman, S. M.; Kröhnert, J.; Jentoft, F. C.; Kemnitz E. *Catal. Today* **2010**, *152*, 2.
20. Coman, S. M.; Parvulescu, V. I.; Wuttke, S.; Kemnitz, E., *ChemCatChem*. **2010**, *2*, 92.
21. Candu, N.; Wuttke, S.; Kemnitz, E.; Coman, S. M.; Parvulescu, V. I. *Appl. Catal. A: Gen.* **2011**, *391*, 169.
22. Troncea, S. B.; Wuttke, S.; Kemnitz, E.; Coman, S. M.; Parvulescu, V. A. *Appl. Catal. B: Environ.* **2011**, *107*, 260.
23. Telleria, I. A.; Hemmann, F.; Jäger, C.; Arias, P. L.; Kemnitz, E. *J. Catal.* **2013**, *305*, 81.
24. Lide D. R., *Handbook of Chemistry and Physics*, CRC Press, **2003-2004**.
25. Li, H.; Niu, N. S.; Lu, C.; Li J. *Fuel* **2016**, *176*, 63.
26. Guo, Y.; Wuttke, S.; Vimont, A.; Daturi, M.; Lavalley, J. C.; Teinz, K.; Kemnitz, E. *J. Mater. Chem.* **2012**, *22*, 14587.